Published in final edited form as:
J Med Chem. 2012 July 26; 55(14): 6512–6522. doi:10.1021/jm300575y.

Synthesis and Nicotinic Acetylcholine Receptor In Vitro and In Vivo Pharmacological Properties of 2'-Fluoro-3'-(substituted phenyl)deschloroepibatidine Analogues of 2'-Fluoro-3'-(4-nitrophenyl)deschloroepibatidine (4-Nitro-PFEB or RTI-7527-102)

Pauline Ondachi[†], **Ana Castro**[‡], **Charles W. Luetje**[‡], **M. Imad Damaj**[§], **S. Wayne Mascarella**[†], **Hernán A. Navarro**[†], and **F. Ivy Carroll**[†,*]

[†]Center for Organic and Medicinal Chemistry, Research Triangle Institute, P. O. Box 12194, Research Triangle Park, North Carolina 27709, United States

[‡]Department of Molecular and Cellular Pharmacology, Miller School of Medicine, University of Miami, Miami, Florida 33101, United States

[§]Department of Pharmacology and Toxicology, P.O. Box 980615, Virginia Commonwealth University Medical Campus, Richmond, Virginia 23298-0524, United States

Abstract

Herein, we report the synthesis and nicotinic acetylcholine receptor (nAChR) in vitro and in vivo pharmacological properties of 2'-fluoro-3'-(substituted phenyl)deschloroepibatidines **5b–g**, analogues of 3'-(4-nitrophenyl) compound **5a**. All compounds had high affinity for the α4β2-nAChR and low affinity for α7-nAChR. Initial electrophysiological studies showed that all analogues were antagonists at α4β2-, α3β4-, and α7-nAChRs. The 4-carbamoylphenyl analogue **5g** was highly selective for α4β2-nAChR over α3β4- and α7-nAChRs. All the analogues were antagonists of nicotine-induced antinociception in the tail-flick test. Molecular modeling docking studies using agonist-bound form of the X-ray crystal structure of the acetylcholine binding protein suggested several different binding modes for epibatidine, varenicline, and **5a**–**5g**. In particular, a unique binding mode for **5g** was suggested by these docking simulations. The high binding affinity, in vitro efficacy, and selectivity of **5g** for α4β2-nAChR combined with its nAChR functional antagonist properties suggest that **5g** will be a valuable pharmacological tool for studying the nAChR and may have potential as a pharmacotherapy for addiction and other CNS disorders.

Keywords

Nicotinic receptors; epibatidine; nicotinic antagonist; α4β2-nAChR selectivity; electrophysiological studies; tail-flick; hot-plate; molecular modeling

Tobacco use is the leading preventable cause of disease, disability, and death in the United States (US). According to the Centers for Disease Control (CDC) 2011 Smoking and Tobacco Use—Fact Sheet,[1] cigarette smoking results in more than 440,000 premature deaths in the US each year—about 1 in every 5 deaths.

*To whom correspondence should be addressed. Phone: 919 541-6679. Fax: 919 541-8868. fic@rti.org.

Supporting Information. Elemental analysis data. This material is available free of charge via the Internet at http://pubs.acs.org.

The continued use of tobacco products is believed to be due in large part to addiction to nicotine (**1**). It is well documented that nicotinic acetylcholine receptors (nAChRs) are the body's targets for nicotine actions. Considerable research suggests that α4β2*-nAChRs, the most abundant subtype in brain, play a central role in nicotine addiction.[2–4] Human genetic association studies have also implicated α3 (CHRNA3), α5 (CHRNA5), and β4 (CHRNB4) nAChR subunits in nicotine-dependent subjects.[5–7] In addition, recent evidence from animal studies suggests that α3β4*-nAChRs may also contribute to nicotine's addictive properties[2–4,8–10] as well as reduction of ethanol consumption.[11] The association of nicotine with both α4β2*- and α3β4*-nAChR in the addictive process makes these receptors attractive targets to combat nicotine addiction.

Even though nicotine dependence has a huge impact on global health, pharmacotherapies for treating tobacco use are limited. FDA-approved therapies include nicotine-replacement therapies (NRTs), bupropion (**2**), and varenicline (**3**). Since only about one-fifth of smokers are able to maintain long-term (12 months) abstinence with any of the present pharmacotherapies,[12,13] new and improved drugs are needed.

During the last few years, we have conducted structure-activity relationship studies (SARs) using the potent nAChR agonist epibatidine (**4**) as a lead structure to identify agonist and antagonist pharmacophores for the nAChR.[14–20] In addition, we hoped that the studies would provide lead structures for the development of pharmacotherapies useful for treating smokers. In one of our studies we identified 2'-fluoro-3'-(4-nitrophenyl)deschloroepibatidine (**5a**), also referred to as RTI-7527-102 and 4-nitro-PFEB, as a very high affinity nAChR ligand, which showed potent antagonism of nicotine-induced antinociception in the tail-flick and hot-plate test.[17] In vitro testing of **5a** showed that it was a competitive antagonist of human α4β2-nAChRs with a potency 17-fold higher than that of dihydro-β-erythroidine (**6**) and lower potency at α3β4- and α7-nAChRs.[21] In addition, the α4β2-nAChR antagonist **5a** attenuated the discriminative stimulus effects of nicotine, reduced nicotine's ability to facilitate intracranial self-stimulation (ICSS), blocked conditioned place preference (CPP) produced by nicotine and dose-dependently blocked i.v. nicotine self-administration in rodents.[22] Thus, **5a** has both in vitro and in vivo properties thought to be favorable for a potential pharmacotherapy to treat smokers. Unfortunately, **5a** has a nitro-substituted phenyl group, a system that is associated with toxicity via partial reduction in vivo to the hydroxylamine, which can undergo metabolic activation to an electrophilic nitroso species. In this study we report the synthesis and nAChR in vitro and in vivo properties of **5b–g**, compounds which have the 4-nitro group in **5a** replaced by other strong electron withdrawing groups. Computational chemistry studies were performed to compare the possible binding interactions of the 4-substituents of **5a–5g** within a model of the nicotinic receptor.

CHEMISTRY

Synthesis of Compounds

Scheme 1 outlines the synthesis used to prepare **5b–e**. Treatment of **7**[17] with di-*tert*-butyl dicarbonate in methylene chloride containing triethylamine at room temperature overnight gives *tert*-butylcarbonyl-protected intermediate **8**. Suzuki cross-coupling of **8** with 4-trifluoromethylphenylboronic acid, 4-methanesulphonylphenylboronic acid, and 4-cyanophenylboronic acid in the presence of palladium diacetate, tris(*o*-tolyl)phosphine, and sodium carbonate in a dimethoxyethane water mixture at 85 °C yielded **9**, **10**, and **11**. In the case of the synthesis of **12**, a Suzuki cross-coupling of **8** was conducted with the 4-boronobenzenesulfonamide through a microwave-assisted reaction in the presence of 1,1'-bis(diphenylphosphino)ferrocine-palladium(II) dichloride [$PdCl_2$(dppf)] as catalyst, potassium carbonate as base, and 1,4-dioxane and water as solvents. The reaction was

irradiated at 140 °C for 20 min to provide **12**. Treatment of **9–12** with trifluoroacetic acid in methylene chloride yielded **5b–e**. The synthesis of **5f** is given in Scheme 2. Suzuki-Miyaura borylation of **8** was performed through a microwave-assisted cross-coupling with bis(pinacolato)diboron in the presence of the weak base potassium acetate and $PdCl_2$(dppf) as catalyst, irradiated at 140 °C for 15 min to furnish the boronic ester **13**. Suzuki cross-coupling of **13** with 4-bromophenyl(trifluoromethyl)sulfone (**15**) [prepared by the oxidation of commercially available 4-bromotrifluoromethylthiobenzene (**14**) with *m*-chloroperoxybenzoic acid (MCPBA)] afforded **16**, which on treatment with trifluoroacetic acid gave **5f**.

Compound **5g** was synthesized as shown in Scheme 3. Tetrakis(triphenylphosphine)palladium-catalyzed coupling of **7** with 4-carbamoylphenylboronic acid in dioxane-water containing potassium carbonate yielded **5g**. It should be noted that **5a–g** are all racemic analogues of epibatidine.

Molecular Modeling

To confirm that the nAChR could accomodate the structure and to explore the possible functional similarities to epibatidine of the proposed target compounds each was examined in a series of ligand-receptor docking simulations. The model of the nAChR epibatidine binding pocket used in these calculations was based on the recently deposited X-ray crystallographic structure of a *Lymnaea stagnalis* acetylcholine binding protein (Ls-AChBP) chimera co-crystallized with epibatidine.[23] AChBP is considered a close structural analogue of nicotinic acetycholine receptors and this humanized Ls-AChCP chimera was selected as it was expected to have greater relevance to the mammalian receptor.

Docking calculations were performed using the Surflex-Dock module of the Tripos Sybyl molecular modeling program suite.[24] This system performs unbiased, conformationally-independent docking of candidate ligands to proteins which allows full flexibility of both the ligand and receptor side-chains. An empirical scoring function (based on the Hammerhead docking system) is used to select likely binding modes and conformations. The scoring function includes steric, polar, entropic, and solvation terms to estimate the binding affinity of each docked ligand.

RESULTS

Biological

The nAChR binding affinities and the functional nicotinic pharmacological properties of 2'-fluoro-3'-(substituted phenyl)deschloroepibatidine analogues **5a–g** were determined. The K_i values for the inhibition of [^{3}H]epibatidine and [^{125}I]iodoMLA binding at the α4β2*- and α7-nAChRs, respectively, for **5b–g** along with reference compounds nat-epibatidine (**4**), varenicline (**3**), and the lead compound **5a** are listed in Table 1. The reference standards nat-epibatidine and varenicline and lead compound **5a** have K_i values of 0.026, 0.12, and 0.009 nM for the α4β2*-nAChR, respectively. Similar to **5a**, **5b–g** with K_i values ranging from 0.03 to 0.94 nM had high affinity for α4β2*-nAChR. The 4-(trifluoromethanesulfonylphenyl) analogue **5f** with a K_i of 0.03 nM had the highest affinity. Similar to lead compound **5a**, **5b–g** had weak affinity for the α7-nAChR (K_i > 2 μM). In a preliminary study using inhibition of [^{3}H]epibatidine and stably transfected nAChR cell lines, Huang et al.[25] reported that **5c** had α4β2-nAChR selectivity relative to five other αβ-nAChRs.

The nAChR subtype selectivity of **5b–g**, as well as nat-epibatidine, varenicline and lead compound **5a**, was assessed in an initial electrophysiological assay using α4β2-, α3β4-, and

α7-nAChRs expressed in *Xenopus* oocytes (Table 1). The current response to a high concentration (100 μM) of each compound was compared to the maximum response that can be achieved with acetylcholine. Compounds **5a–f** lacked agonist activity at α4β2 in this initial screen, while **5g** had a low level of agonist activity at this subtype. Compounds **5b** and **5d–e** lacked agonist activity at α3β4, while **5a**, **5c**, **5f**, and **5g** had a low level of agonist activity at this subtype. At α7 nAChRs, **5a–f** displayed low levels of agonist activity, while **5g** showed a moderate level of agonist activity (17 ± 4% of the maximal ACh response). As an initial screen of antagonist properties, we measured the current response to an EC_{50} concentration of acetylcholine in the presence of 100 μM of each compound and compared this to a preceding current response to acetylcholine alone. Compounds **5a–g** were found to be antagonists at the α4β2-, α3β4-, and α7-nAChR subtypes. The results from this initial screen suggested that this compound series manifested a variety of desirable functional selectivities: α4β2- and α3β4- over α7-nAChR and α4β2-over α3β4- and α7-nAChR. We examined the subtype selectivity of antagonist activity for for some of these compounds (**5a–d** and **5g**) in more detail by generating concentration-inhibition curves (Table 2). Compound **5b** showed no selectivity among α4β2-, α3β4-, and α7-nAChRs. Compounds **5a** and **5d** showed a moderate selectivity for α4β2- over α3β4-nAChR (2.5-fold and 4-fold, respectively) and a greater selectivity for α4β2- over α7-nAChR (10-fold in each case). Compound **5c** showed similar antagonist potency at α4β2 and α3β4 and was less potent at α7 (9-fold and 14-fold, respectively). Compound **5g** was highly selective for α4β2- over α3β4- and α7-nAChR (23-fold, in each case).

Similar to varenicline, the lead compound **5a** had no functional activity in the mouse tail-flick and hot-plate tests but had agonistic effects with ED_{50} values of 0.21 and 0.22 mg/kg in the hypothermia and spontaneous activity assays compared to 2.8 and 2.1 mg/kg in these two tests for varenicline. None of the analogues **5b–g** had activity in the tail-flick and hot-plate tests. Analogues **5b**, **5c**, **5d**, and **5e** also had no activity in the hypothermia and spontaneous activity test. Analogue **5f** was only active in the spontaneous activity test. Similar to **5a** and varenicline, **5g** was only active in the hypothermia and spontaneous activity tests. The discrepancy between the high binding affinity of **5a–g** for α4β2*-nAChRs and their absence of agonistic effects in the pain tests suggests that these compounds might act as functional nAChR antagonists in the two pain tests. Indeed all the compounds were antagonists of nicotine-induced antinociception in the tail-flick test with AD_{50} values ranging from 0.9 μg/kg for **5e** to 38 μg/kg for **5b**. Compounds **5b**, **5d**, and **5e** were also antagonists in the hot-plate test. Compound **5e** with AD_{50} values of 0.9 in the tail-flick test was more potent than **5a** in this assay. Overall these acute mouse results suggest that **5b**, **5c**, **5d**, and **5e** are nAChR antagonists, and **5a**, **5g**, and **5f** are weak partial agonists.

Molecular Modeling

The results of these docking studies for **5a–5g** (CPK atom-type coloring scheme) and varenicline ("Var") compared to the observed binding mode of epibatidine ("Epi") are show in Figure 1. The "total" docking scores (an estimated −log(Kd), as calculated with the Tripos CScore module, were used to select the optimal binding geometries. The CScore "total" docking scores for this series were **5a**, 7.55; **5b**, 7.53; **5c**, 6.74; **5d**, 7.36; **5e**, 9.02; **5f**, 7.46; and **5g**, 9.40. All of the observed and predicted binding geometries share a common feature: the cationic azabicyclic ring of each ligand is centered in the electron-rich pocket formed by a cluster of five aromatic residues (A/TYR 91, A/TRP145, A/TYR184, A/TYR191, B/TRP 53). (This binding pocket is also bordered by the hydrophobic A/CYS186 - A/CYS187 and B/LEU116 residues.) In addition, a hydrogen-bond interaction within the aromatic pocket between the ligand and either A/TRP145 (backbone carbonyl) or the adjacent A/TYR91 (sidechain hydroxyl) is observed or predicted for all ligands (the observed structure of the epibatidine-receptor complex and the computationally-docked varenicline binding geometry

exhibit both). By pivoting around these common anchoring interactions, four distinct binding modes are exhibited (by epibatidine) or predicted (for **5a–5g** and varenicline). In binding mode 1, the smaller ligands, epibatidine and varenicline, associate with a relatively small pocket formed by B/LEU116, B/GLN114, B/LEU106, and A/TRP146 (Figure 2A). Compounds **5a–5g** are too large to fit into this pocket and thus are predicted to interact with the receptor differently than the parent compound epibatidine or varenicline. In binding mode 2 (Figure 2B), compounds **5a**, **5c**, and **5d** associate with the aforementioned aromatic pocket and, in addition, the ligand polar substituents interact with a relatively polar receptor pocket bordered by B/SER162, B/GLY163, B/ASP160, and B/SER34. In the case of **5a**, additional hydrogen-bond interactions with B/GLY163 and B/GLN55 are suggested by the docking simulation. A hydrogen-bond interaction between the ligand pyridinyl nitrogen and B/GLN55 is also predicted for compound **5c**. Compounds **5b**, **5e**, and **5f** are predicted to have a slightly different binding mode (Figure 2C) where the para-substituent is situated in the large cavity between the base of the C-loop and B/SER162. In this set of three epibatidine analogs, additional hydrogen-bonds are predicted involving B/GLY163 (**5e** and **5f**) and A/TRP45, B/SER162, B/163, and B/GLN55 (**5f**). A unique, fourth binding mode is predicted for compound **5g** (Figure 2D). The docking simulation for this compound predicts that the 4-acetamido substituent will be situated in a polar pocket bordered by B/SER32, B/ASP160, and B/GLN55 where it forms a salt-bridge with B/ASP160. This interaction, unique to **5g**, accounts for the very favorable predicted pKd of 9.40, the highest for the series.

DISCUSSION

In previous studies we showed that the addition of a 3'-substituent to epibatidine, 2'-fluoroepibatidine, or deschloroepibatidine provided analogues with different degrees of nAChR functional agonist and antagonist properties.[14–17,19,26] All 2'-fluoro-3'-(substituted phenyl)deschloroepibatidine analogues possessed high affinity for α4β2*-nAChRs. Compound **5a**, with a K_i = 0.009 nM compared to a K_i = 0.026 nM for nat-epibatidine, had the highest affinity.[17] Thus, a bulky substituted phenyl group at the 3'-position does not interfere with receptor recognition for the α4β2*-nAChRs. All analogues were potent antagonists. Thus, a 2'-fluoro group on the pyridine ring combined with bulky 3'-substituents interferes with receptor activation. Several 2'-fluoro-3'-(substituted phenyl)deschloroepibatidine analogues were evaluated for α4β2 potency and selectivity in cloned nAChRs.[21] The 3'-(4-nitrophenyl) analogue **5a** was a more potent and selective competitive antagonist for the α4β2-nAChR than dihydro-β-erythroidine (**6**, DHβE). Compound **5a** was also evaluated in several animal models related to nicotine reward and reinforcement: drug discrimination (DD), intracranial self-stimulation (ICSS), conditioned place preference (CPP), and limited access to nicotine i.v. self-administration (SA).[22] All of these behavioral effects of nicotine are largely mediated by neuronal α4β2*-nAChRs. The antagonist **5a** attenuated the DD effect of nicotine but alone failed to produce nicotine-like DD effects, reduced nicotine's ability to facilitate ICSS while producing no effects on ICSS alone, and blocked CPP produced by nicotine but alone failed to produce a CPP and dose-dependently blocked SA.[22] Results from these studies showed that **5a** has the nAChR in vitro and in vivo pharmacological properties for a potential clinical candidate to treat nicotine dependence. Since **5a** has an aromatic nitro substituent that could be partially reduced to a hydroxyamine group in vivo which could undergo metabolite activation to an electrophlic nitroso species resulting in toxic effects, its potential for drug development could be questioned. In this study we designed, synthesized, and evaluated the **5a** analogues **5b–g** for their in vitro and in vivo nAChR properties. Similar to lead structure **5a**, each compound has a strong electron withdrawing 4-substituent on the 3'-aryl group. Table 3 lists the σ constants for **5a–g**.[27]

We evaluated the potency and selectivity of **5a–g** in vitro using three cloned nAChR subtypes (α4β2, α3β4 and α7) expressed in *Xenopus* oocytes and assayed using electrophysiology. While we found lead structure **5a** to be selective for α4β2 over α3β4, the difference in potency (2.5-fold) was much less than previously reported.[21] In our electrophysiology assay in the current study, we used rat nAChR subunits to generate the nAChRs. In the previous study, human α4β2 was compared to rat α3β4.[21] Thus, the difference in selectivity may be attributable to a difference between rat and human α4β2. Such pharmacological differences have been previously reported for rat and human α7.[28] Concentration-inhibition analysis showed **5b** to be non-selective for the nAChR subtypes tested. Compound **5d** was modestly selective for α4β2 over α3β4 and α7, while **5c** was moderately selective for α4β2 and α3β4 over α7. Interestingly, the greatest subtype selective was generated by placing a carbamoyl moiety at the 4 position (**5g**). Compound **5g** displayed 23-fold selectivity for α4β2 over α3β4 and α7. Molecular modeling docking studies of **5g** to the antagonist form of the AChBP suggests a binding mode that could account for the α4β2-nAChR selectivity of **5g**.

While the functional selectivity of compound **5g** for α4β2 over α7 is exciting, the degree of selectivity (23-fold) observed in the electrophysiological assay is much less than what we observed in the radioligand binding assays (>15,000-fold). Similarly, while compounds **5a–d** showed a selectivity of three to four orders of magnitude for α4β2 over α7 in radioligand binding assays, these compounds displayed only moderate selectivity (6- to 10-fold for **5a, 5c**, and **5d**) or no selectivity (**5b**) in the electrophysiology assay. These finding are reminiscent of what was observed when comparing results for varenicline in radioligand binding and electrophysiological assays.[29,30] The reason for this difference is equilibrium binding assays and electrophysiological assays are measuring the properties of different receptor states. Unfortunately, the large differences in affinity observed in equilibrium binding assays are generally not observed in functional assays and the rank order of affinities do not necessarily correlate with the rank orders of functional potency.[31,32]

In summary several 2'-fluoro-3'-(substituted phenyl)deschloroepibatidine analogues were developed which had high binding affinity for the α4β2-nAChR. The high binding affinity and in vitro efficacy selectivity of the 3'-(4-carbamoylphenyl) analogue **5g** combined with its ability to antagonize nicotine-induced antinociception in the tail-flick test suggest that this compound will be a valuable pharmacological tool for studying the nAChR and may have potential as a pharmacotherapy for addiction and other CNS disorders. In addition, having these various compounds with a variety of selectivity profile toward both α4β2- and α3β4-nAChR subtypes relative to the α7-nAChR provides the opportunity for manipulating these important pharmacological and therapeutical targets and allows for the evaluation of dual-acting nicotinic antagonists.

EXPERIMENTAL SECTION

Melting points were determined on a Mel-temp (Laboratory Devices, Inc.) capillary tube apparatus. Nuclear magnetic resonance (^{1}H and ^{13}C NMR) spectra were recorded at 300 MHz (Bruker Avance 300). Chemical shift data for the proton resonances were reported in parts per million (δ) relative to tetramethylsilane (δ 0.0) as internal standard. Thin-layer chromatography was carried out on Whatman silica gel 60 plates. Visualization was accomplished under UV or in an iodine chamber. Microanalysis was carried out by Atlantic Microlab, Inc. Purity of compounds (>95%) was established by elemental analysis. Flash chromatography was carried out using a CombiFlash Rf Teledyne Isco instrument and columns, silica gel 60 (230–400 mesh), and various solvent mixtures. Microwave reactions were carried out using a CEM Discover Microwave Reactor.

The [^{3}H]epibatidine was purchased from Perkin Elmer Inc. (Boston, MA). The [^{125}]iodo-MLA was synthesized as previously reported.[33]

General Procedure for the Synthesis of Compounds 5b and 5c Hydrochlorides

The respective Boc-protected compound (**9** or **10**) (0.7 mmol) was dissolved in anhydrous CH_2Cl_2 (3 mL) and cooled in ice-water bath. TFA (3 mL) was added over a 30-min period and was stirred at r.t. for 1 h. The mixture was poured into a cold solution of NH_4OH in water (1:1) and was extracted with CH_2Cl_2. The organic phase was washed with brine, dried (Na_2SO_4), and evaporated to dryness. The resulting residue was subjected to flash chromatography on a silica gel column using CH_2Cl_2–MeOH as the eluent to provide the respective amine (**5b** or **5c**). Subsequently, the free base was dissolved in MeOH (5 mL) at room temperature, HCl (1M in ether) added with a syringe pump over 50 min at room temperature, stirred for 30 min, and the solvent removed. The resulting residue was recrystallized from MeOH–ether to provide the hydrochloride salt.

2'-Fluoro-3'-(4'-trifluoromethylphenyl)deschloroepibatidine (5b) Hydrochloride—^{1}H NMR of **5b** ($CDCl_3$) δ (ppm) 1.5–1.7 (m, 5H), 1.8–1.9 (m, 1H), 2.83 (dd, 1H, *J* = 5.1, 9.0 Hz), 3.62 (br s, 1H), 3.81 (br s, 1H), 7.70 (s, 4H), 8.06 (dd, 1H, *J* = 2.4, 3.6 Hz), 8.13 (m, 1H); ^{13}C NMR ($CDCl_3$) δ (ppm) 29.6, 30.6, 31.8, 40.9, 44.7, 56.8, 63.2, 125.9 (q, *J* = 15 Hz), 129.6 (d, *J* = 12.3 Hz), 140.2 (d, *J* = 14.7 Hz), 141.4 (d, *J* = 18.6 Hz), 146.1 (d, *J* = 57.6 Hz), 157.7, 160.8, 162.7.

Compound **5b**•HCl was obtained as a yellow solid. *Anal.* ($C_{18}H_{17}ClF_4N_2$•H_2O): C, H, N.

2'-Fluoro-3'-(4-cyanophenyl)deschloroepibatidine (5c) Hydrochloride—^{1}H NMR of **5b** ($CDCl_3$) δ (ppm) 1.5–1.7 (m, 5H), 1.8–1.9 (m, 1H), 2.84 (dd, 1H, *J* = 5.1, 9.0 Hz), 3.61 (br s, 1H), 3.82 (m, 1H), 7.6–7.8 (m, 4H), 8.09 (dd, 1H, *J* = 2.4, 6.6 Hz), 8.14 (m, 1H); ^{13}C NMR ($CDCl_3$) δ (ppm) 29.6, 30.7, 31.9, 40.9, 44.6, 56.8, 63.2, 112.3, 118.9, 121.5 (d, *J* = 112.2 Hz), 129.9 (d, *J* = 13.2 Hz), 132.7, 139.3, 140.1, 141.6, 146.5 (d, *J* = 57.9 Hz), 157.5, 160.7.

Compound **5c**•HCl as a yellow solid. *Anal.* ($C_{18}H_{17}ClFN_3$•$0.5H_2O$): C, H, N.

2'-Fluoro-3'-(4-methanesulfonylphenyl)deschloroepibatidine (5d) Hydrochloride—Compound **11** (312 mg, 0.7 mmol) was dissolved in anhydrous CH_2Cl_2 (3 mL) and cooled in an ice-water bath. TFA (3 mL) was added in 30 min. After stirring at room temperature for 1 h, the mixture was poured into a cold solution of NH_4OH in water (1:1). The mixture was then extracted with CH_2Cl_2. The organic phase was washed with brine, dried (Na_2SO_4), and evaporated to dryness. Flash chromatography on a silica gel column with CH_2Cl_2–MeOH gave 242 mg (99%) of the free base **5d** as a clear oil: ^{1}H NMR ($CDCl_3$) δ (ppm) 1.5–1.7 (m, 5H), 1.8–1.9 (m, 1H), 2.87 (dd, 1H, *J* = 5.1, 9.0 Hz), 3.11 (s, 3H), 3.65 (br s, 1H), 3.84 (m, 1H), 7.7–7.8 (m, 2H), 8.0–8.05 (m, 2H), 8.09 (dd, 1H, *J* = 2.4, 3.6 Hz), 8.15 (m, 1H); ^{13}C NMR ($CDCl_3$) δ (ppm) 29.6, 30.5, 31.7, 40.8, 44.6, 44.9, 56.8, 63.2, 121.6 (d, *J* = 112.5 Hz), 128.0, 130.2 (d, *J* = 12.3 Hz), 140.3 (d, *J* = 14.7 Hz), 141.3 (d, *J* = 18.6 Hz), 146.6 (d, *J* = 57.6 Hz), 157.6, 160.8.

The free base **5d** (242 mg, 0.7 mmol) was dissolved in MeOH (7 mL) at room temperature. HCl (1M in ether, 7 mL) was added with a syringe pump over 50 min at room temperature. After stirring for 30 min, the solvent was removed. The residue was recrystallized from MeOH–ether to give **5d**•HCl as a yellow solid. *Anal.* ($C_{18}H_{20}ClFN_2O_2S$•$0.75H_2O$): C, H, N.

2'-Fluoro-3'-(4-aminosulfonylphenyl)deschloroepibatidine (5e) Hydrochloride—A solution of **12** (245 mg, 0.55 mmol) in CH_2Cl_2 (3 mL) and TFA (1 mL) was stirred at room temperature for 2 h. The solvent was removed under reduced pressure, and the residual was treated with a 20 mL solution of $NH_4OH–H_2O$ (3:1). The organic product was extracted with $CHCl_3$ (3 × 30 mL), dried over anhydrous sodium sulfate, filtered through Celite, and concentrated in vacuo. Purification of the residual by flash chromatography through an ISCO column provided 159 mg (84%) of **5e** as a colorless oil: ^{1}H NMR (CD_3OD) δ (ppm) 1.48–1.80 (m, 5H), 2.02–2.09 (dd, J = 9.1, 12.3 Hz, 1H), 3.02–3.07 (dd, J = 4.8, 8.9 Hz, 1H), 3.67 (s, 1H), 3.76 (s, 1H), 7.78 (dd, J = 1.5, 8.5 Hz, 2H), 7.91 (dd, J = 8.6, 1.9 Hz, 2H), 8.06 (dd, J = 2.4, 9.5 Hz, 1H), 8.14 (s, 1H); ^{13}C NMR (CD_3OD) δ (ppm) 29.9, 31.8, 41.0, 45.7, 57.9, 63.6, 104.6, 123.7 (J_{CF} = 28.2 Hz), 127.5, 130.6, 130.6, 137.4 (J_{CF} = 4.6 Hz), 141.5 (J_{CF} = 3.1 Hz), 145.1, 146.7 (J_{CF} = 14.6 Hz), 153.0, 157.6; MS (ESI) m/z 348.1 $(M+H)^+$.

The free base **5e** was converted to **5e**•HCl using HCl in diethyl ether: mp 205–208 °C; ^{1}H NMR (methanol-d_4) δ (ppm) 1.87–2.19 (m, 5H), 2.45–2.53 (dd, J = 9.6, 13.4 Hz, 1H), 3.51–3.56 (dd, J = 4.8, 8.9 Hz, 1H), 4.33 (s, 1H), 4.55 (s, 1H), 7.81 (dd, J = 1.5, 8.5 Hz, 2H), 8.01 (dd, J = 1.8, 6.8 Hz, 2H), 8.09 (dd, J = 2.4, 9.1 Hz, 1H), 8.22 (s, 1H); ^{13}C NMR (methanol-d_4) δ (ppm) 27.0, 29.1, 37.8, 43.4, 60.4, 64.3, 103.0, 123.2, 127.6, 130.7, 130.8, 137.6, 138.7, 141.6, 145.1, 146.7 (J_{CF} = 14.0 Hz), 159.0, 162.2; MS (ESI) m/z 348.1 $[(M\text{-}HCl))^+$, M = $C_{16}H_{18}FN_3O_2S$]. *Anal.* ($C_{17}H_{18}ClFN_3O_2S•H_2O$): C, H, N.

2'-Fluoro-3'-(4-trifluoromethanesulfonylphenyl)deschloroepibatidine (5f) Hydrochloride—A solution of **16** (308 mg, 0.62 mmol) in CH_2Cl_2 (3 mL) and TFA (1 mL) was stirred at room temperature for 2 h. The solvent was removed under reduced pressure, and the residual was treated with a 20 mL solution of $NH_4OH–H_2O$ (3:1). The organic product was extracted with $CHCl_3$ (3 × 30 mL), dried over anhydrous sodium sulfate, filtered through Celite, and concentrated in vacuo. Purification of the residual by flash chromatography through an ISCO column provided 202 mg (82%) of **5f** as a colorless oil: ^{1}H NMR ($CDCl_3$) δ (ppm) 1.55–1.69 (m, 7H), 1.93–2.05 (dd, J = 9.0, 12.4 Hz, 1H), 2.83–2.87 (dd, J = 4.8, 8.9 Hz, 1H), 3.61 (s, 1H), 3.84 (s, 1H), 7.88 (dd, J = 1.4, 8.5 Hz, 2H) 8.11–8.19 (m, 4H); ^{13}C NMR ($CDCl_3$) δ (ppm) 30.4, 31.56, 40.7, 44.3, 56.4, 62.9, 117.6, 120.4 (J_{CF} = 28.2 Hz), 122.0, 130.2, 130.3, 131.0, 140.0 (J_{CF} = 3.4 Hz), 141.5 (J_{CF} = 4.7 Hz), 143.0 (J_{CF} = 5.6 Hz), 146.8 (J_{CF} = 14.7 Hz), 157.2, 160.3; MS (ESI) m/z 401.2 $(M+H)^+$.

The free base **5f** was converted to **5f**•HCl using HCl in diethyl ether: mp 144–148 °C; ^{1}H NMR (methanol-d_4) δ (ppm) 1.85–2.22 (m, 5H), 2.47–2.54 (dd, J = 9.6, 13.4 Hz, 1H), 3.53–3.58 (dd, J = 4.8, 8.9 Hz, 1H), 4.35 (s, 1H), 4.61 (s, 1H), 8.07 (dd, J = 1.4, 8.6 Hz, 2H) 8.16 (dd, J = 2.4, 9.3 Hz, 1H), 8.21 (d, J = 8.4 Hz, 2H), 8.29 (s, 1H); ^{13}C NMR (methanol-d_4) δ (ppm) 26.8, 28.9, 37.6, 43.3, 60.5, 64.3, 119.1, 122.2 (J_{CF} = 28.2 Hz), 123.4, 132.0, 132.3, 137.5, 141.8, 143.9 (J_{CF} = 5.2 Hz), 147.9 (J_{CF} = 14.8 Hz), 158.9, 162.1; MS (ESI) m/z 401.0 $[(M\text{-}HCl))^+$, M = $C_{18}H_{16}F_4N_2O_2S$]. *Anal.* ($C_{18}H_{16}ClF_4N_2O_2S•H_2O$): C, H, N.

2'-Fluoro-3'-(4-carbamoylphenyl)deschloroepibatidine (5g) Hydrochloride—A solution of **7** (178 mg, 0.66 mmol), 4-carbamoylphenyl boronic acid (130 mg, 0.79 mmol), $Pd(PPh_3)_4$ (38 mg, 5 mol %), and K_2CO_3 (182 mg, 1.31 mmol) in 1,4-dioxane (5 mL) and H_2O (0.8 mL) in a sealed tube was degassed through bubbling N_2 for 20 min then heated at 100 °C for 20 h. After cooling to room temperature, the solvent was removed in vacuo, and the residue was redissolved in EtOAc. Water (20 mL) was added and the organic product extracted with EtOAc (3 × 30 mL). The combined organic layers were dried ($MgSO_4$), filtered through Celite, and concentrated in vacuo. The crude residue was purified on silica gel ($CHCl_3$–MeOH) by flash chromatography to provide 160 mg (78% yield) of **5g** as a colorless oil: ^{1}H NMR ($CDCl_3$) δ 1.53–1.72 (m, 5H), 1.91–1.98 (m, 3H), 2.82–2.86 (m,

1H), 3.61(s, 1H), 3.80 (s, 1H), 6.58 (br s, 2H), 7.62–7.65 (m, 2H), 7.89–7.92 (m, 2H), 8.01 (dd, *J* = 2.4, 9.6 Hz, 1H), 8.10 (s, 1H); ^{13}C NMR ($CDCl_3$) δ 30.2, 40.5, 44.4, 56.4, 62.8, 122.2, 127.1, 129.0, 133.1, 137.8, 139.8, 140.8, 145.6, 160.5, 169.1; MS (ESI) m/z 312.6 $(M+H)^+$.

A solution of **5g** in chloroform in a vial was treated with a solution of HCl in diethyl ether. The excess solvent was removed in vacuo to give **5g**•HCl: mp 202–206 °C; ^{1}H NMR (CD_3OD) δ 1.91–2.20 (m, 5H), 2.46–2.54 (dd, *J* = 3.8, 9.6 Hz, 1H), 3.51–3.56 (m, 1H), 4.35, (d, *J* = 3.5 Hz, 1H), 4.60 (d, *J* = 2.5 Hz, 1H), 7.77–7.74 (m, 2H), 7.99–8.02 (m, 2H), 8.10 (dd, *J* = 2.4, 9.2 Hz, 1H), 8.20 (s, 1H); ^{13}C NMR (CD_3OD) δ 26.8, 28.9, 37.6, 43.3, 60.5, 64.3, 123.8, 129.1, 130.2, 135.0, 137.2, 138.3, 141.4, 146.4, 159.1, 162.3, 171.6; MS (ESI) m/z 312.4 $(M+H)^+$. *Anal.* ($C_{18}H_{19}ClFN_3O$•1.75 H_2O): C, H, N.

7-*tert*-Butoxycarbonyl-2-*exo*-(2'-fluoro-3'-bromo-5'-pyridinyl)-7-azabicyclo[2.2.1]heptane (8)—A solution of **7** (447 mg, 1.65 mmol) in CH_2Cl_2 (15 mL) and Et_3N (350 μL) was treated with $(Boc)_2O$ (540 mg, 2.47 mmol) and stirred overnight. The reaction mixture was then diluted with an additional CH_2Cl_2 (20 mL) and washed with brine. The organic phase was dried over anhydrous Na_2SO_4 and concentrated *in vacuo*. The resultant residue was purified by flash chromatography, and the title compound was isolated as a yellow oil (591 mg, 97%). ^{1}H NMR ($CDCl_3$) δ (ppm) 7.8–8.0 (2H, m), 4.33 (br s, 1H), 4.11 (br s, 1H), 2.83 (dd, 1H, *J* = 4.8, 9.0 Hz), 1.96 (dd, 1H, *J* = 9.0, 12.3 Hz), 1.4–1.8 (5H, m), 1.39 (9H, s); ^{13}C NMR ($CDCl_3$) δ (ppm) 160.2, 157.1, 144.9 (d, *J* = 21.9 Hz), 142.7 (d, *J* = 6.9 Hz), 141.2 (d, *J* = 19.8 Hz), 62.2, 56.3, 44.8, 40.8, 30.0, 29.1, 28.6.

General Procedure for Synthesis of Compounds 9–11

Compound **8** (0.7 mmol) was cross-coupled with the respective boronic acid (1.4 mmol), [4-trifluoromethylphenyl, 4-cyanophenyl, or 4-methanesulphonylphenylboronic acid] in the presence of $Pd(OAc)_2$ (0.07 mmol), tris(*o*-tolyl)phosphine (0.14 mmol) and Na_2CO_3 (1.7 mmol) mixed in DME (2 mL) and H_2O (0.5 mL). The mixture was purged with argon, sealed, and heated in an 85 °C oil bath overnight. After cooling, the mixture was filtered through Celite and washed with EtOAc. The organic phase was washed with brine, dried (Na_2SO_4), and concentrated in vacuo. The residue was purified by flash chromatography on a silica gel column using EtOAc–hexanes as the eluent.

7-*tert*-Butoxycarbonyl-2-*exo*-(2′-fluoro-3′-(4-trifluoromethyl-phenyl)-5′-pyridinyl)-7-azabicyclo[2.2.1]heptane (9)—^{1}H NMR ($CDCl_3$) δ (ppm) 1.43 (s, 9H), 1.5–1.9 (m, 5H), 2.02 (m, 1H), 2.98 (dd, 1H, *J* = 4.8, 9.0 Hz), 4.25 (br s, 1H), 4.41 (br s, 1H), 7.70 (s, 4H), 7.91 (dd, 1H, *J* = 2.4, 6.3 Hz), 8.10 (m, 1H); ^{13}C NMR ($CDCl_3$) δ (ppm) 28.3, 28.9, 29.7, 40.7, 44.8, 56.1, 62.1, 80.0, 125.6 (q, *J* = 15 Hz), 129.3 (d, *J* = 12.6 Hz), 137.9 (d, *J* = 18.6 Hz), 139.4 (d, *J* = 15.3 Hz), 140.0 (d, *J* = 19.5 Hz), 145.7 (d, *J* = 58.2 Hz), 155.0, 157.5, 160.7.

7-*tert*-Butoxycarbonyl-2-*exo*-(2′-fluoro-3′-(4-cyanophenyl)-5′-pyridinyl)-7-azabicyclo[2.2.1]heptane (10)—^{1}H NMR ($CDCl_3$) δ (ppm) 1.43 (s, 9H), 1.5–1.9 (m, 5H), 2.02 (m, 1H), 2.99 (dd, 1H, *J* = 4.8, 9.0 Hz), 4.25 (br s, 1H), 4.41 (br s, 1H), 7.6–7.8 (m, 4H), 7.92 (dd, 1H, *J* = 2.4, 9.6 Hz), 8.12 (m, 1H); ^{13}C NMR ($CDCl_3$) δ (ppm) 28.6, 29.2, 30.0, 41.0, 45.0, 56.3, 62.3, 80.3, 112.4, 116.7, 118.8, 121.7 (d, *J* = 112.5 Hz), 129.8 (d, *J* = 12.9 Hz), 132.7, 139.1, 139.5, 140.4, 146.5 (d, *J* = 58.2 Hz), 155.3, 157.6, 160.8.

7-*tert*-Butoxycarbonyl-2-*exo*-(2′-fluoro-3′-(4-methanesulfonyl-phenyl)-5′-pyridinyl)-7-azabicyclo[2.2.1]heptane (11)—^{1}H NMR ($CDCl_3$) δ (ppm) 1.58 (s, 9H), 1.5–1.9 (m, 5H), 2.02 (m, 1H), 3.00 (dd, 1H, *J* = 4.8, 9.0 Hz), 3.12 (s, 3H), 4.25 (br s, 1H),

4.41 (br s, 1H), 7.7–7.8 (m, 2H), 7.93 (dd, 1H, J = 2.4, 9.6 Hz), 8.0–8.1 (m, 2H), 8.13 (m, 1H); ^{13}C NMR ($CDCl_3$) δ (ppm) 28.6, 29.2, 30.0, 41.0, 44.9, 45.0, 56.4, 62.4, 80.3, 116.4, 121.8 (d, J = 58.2 Hz), 128.1, 130.1 (d, J = 13.2 Hz), 139.7, 140.0, 140.4, 146.5 (d, J = 58.8 Hz), 155.4, 157.7, 160.9.

7-*tert*-Butoxycarbonyl-2-*exo*-(2′-fluoro-3′-(4-benzenesulfonamide)-5′-pyridinyl)-7-azabicyclo[2.2.1]heptane (12)—A solution of **8** (488 mg, 1.32 mmol), 4-boronobenzenesulfonamide (318 mg, 1.58 mmol), $PdCl_2$(dppf) (48 mg, 0.066 mmol), and K_2CO_3 (547 mg, 3.96 mmol) in 1,4-dioxane (3 mL) and H_2O (1 mL) was placed in a microwave vial and degassed through bubbling nitrogen for 20 min. The reaction mixture was then irradiated in a CEM Corporation microwave reactor for 20 min at 140 °C. After cooling to room temperature, the mixture was diluted with 10 mL $CHCl_3$–MeOH (10:1) solution and decanted into a 10 mL aqueous solution of $NaHCO_3$. The organic product was extracted with chloroform (3 × 20 mL), and the combined organic layers were dried (Na_2SO_4), filtered through Celite, and concentrated in vacuo. The resultant residue was purified by flash chromatography through an ISCO column to furnish 245 mg (41%) of **12** as a foamy solid: ^{1}H NMR ($CDCl_3$) δ (ppm) 1.41 (s, 9H), 1.53–1.66 (m, 2H), 1.81–1.93 (m, 3H), 1.98–2.09 (dd, J = 9.0, 12.4 Hz, 1H), 2.95–3.00 (dd, J = 4.8, 8.9 Hz, 1H), 4.24 (s, 1H), 4.40 (s, 1H), 5.47 (s, 2H), 7.67 (dd, J = 1.4, 8.5 Hz, 2H), 7.91 (dd, J = 9.6, 2.4 Hz, 1H), 7.98 (dd, J = 1.9, 8.6 Hz, 2H), 8.10 (s, 1H); ^{13}C NMR ($CDCl_3$) δ (ppm) 28.3 (3C), 28.8, 29.6, 40.4, 44.7, 56.0, 61.9, 80.1, 121.4 (J_{CF} = 28.2 Hz), 126.6, 129.4, 129.4, 138.2 (J_{CF} = 5.2 Hz), 139.5 (J_{CF} = 3.7 Hz), 140.0 (J_{CF} = 4.8 Hz), 142.2 145.6, (J_{CF} = 15.0 Hz), 155.0, 157.3, 160.5.

7-*tert*-Butoxycarbonyl-2-*exo*-(2′-fluoro-3′-(4,4,5,5-tetramethyl-1,3,2-dioxaborolan-2-yl)-5′-pyridinyl)-7-azabicyclo[2.2.1]heptane (13)—In a microwave vial was placed **8** (214 mg, 0.578 mmol, 1.0 equiv), bis(pinacolato)diboron (176 mg, 0.694 mmol, 1.2 equiv), KOAc (170 mg, 1.73 mmol, 3.0 equiv), $PdCl_2$(dppf) (21 mg, 0.0289 mmol, 5 mol %), and anhydrous 1,4-dioxane (3 mL). The mixture was degassed through bubbling nitrogen for 20 min followed by irradiation in a microwave at 140 °C for 20 min. After cooling to room temperature, the mixture was diluted with EtOAc, filtered through a plug of Celite and anhydrous Na_2SO_4, and concentrated in vacuo. The resultant residue was purified by flash chromatograph through a Teledyne ISCO column (EtOAc–hexanes) to provide 589 mg (94%) of **13** as a colorless oil: ^{1}H NMR ($CDCl_3$) δ (ppm) 1.26 (s, 12H), 1.44 (s, 9H), 1.60–1.53 (m, 2H), 1.75–1.92 (m, 3H), 1.96–2.03 (dd, J = 9.0, 12.4 Hz, 1H), 2.87–2.92 (dd, J = 4.8, 8.9 Hz, 1H), 4.19 (s, 1H), 4.40 (s, 1H), 8.07 (dd, J = 8.4, 2.4 Hz, 1H), 8.17 (d, J = 2.7 Hz, 1H); ^{13}C NMR ($CDCl_3$) δ (ppm) 24.8, 28.3 (3C), 28.8, 29.8, 40.2, 44.9, 61.8, 79.7, 84.3, 138.2 (J_{CF} = 5.0 Hz), 146.8, 149.2 (J_{CF} = 15.0 Hz), 154.9, 164.2, 167.4; MS (ESI) m/z 419.7 $(M+H)^+$.

1-Bromo-4-[(trifluoromethyl)sulfonyl]benzene (15)—A stirred ice-cold solution of 4-bromophenyltrifluoromethylsulfide (**14**) (1.5 g, 5.83 mmol) in CH_2Cl_2 (40 mL) was treated with mCPBA (5.03g, 29.2 mmol), and the reaction mixture was allowed to warm to room temperature. Stirring was continued overnight after which the reaction mixture was diluted with additional CH_2Cl_2 (60 mL), washed sequentially with an aqueous saturated $NaHCO_3$ solution (50 mL) and brine (50 mL). The organic layer was dried over anhydrous $MgSO_4$, filtered through Celite, and concentrated in vacuo to provide 1.12g (67%) of **15** as a white crystalline solid that was used without further purification.

7-*tert*-Butoxycarbonyl-2-*exo*-(2′-fluoro-3′-(4-rifluoromethanesulfonyl-phenyl)-5′-pyridinyl)-7-azabicyclo[2.2.1]heptane (16)—A solution of the boronic ester **13** (480 mg, 1.15 mmol), **15** (431 mg, 1.49 mmol), $Pd(PPh_3)_4$ (133 mg, 0.115 mmol),

and K_2CO_3 (462 mg, 3.34 mmol) in DME–EtOH–H_2O (3.2 mL/0.8 mL/1 mL) was placed in a microwave vial and degassed through bubbling nitrogen for 20 min. The mixture was irradiated in a CEM Corporation microwave reactor for 20 min at 140 °C. After cooling to room temperature, the solvent was removed under reduced pressure, and the residue was redissolved in CH_2Cl_2 (10 mL), and H_2O (10 mL) was added. The organic product was extracted with CH_2Cl_2 (3 × 20 mL), and the combined organic layers were dried (Na_2SO_4) and filtered through Celite, and the solvent was removed *in vacuo*. The resultant residue was purified by flash chromatography through a Teledyne ISCO column to furnish 408 mg (71%) of **16** as a colorless oil: ^{1}H NMR ($CDCl_3$) δ (ppm) 1.43 (s, 9H), 1.55–1.68 (m, 2H), 1.82–1.92 (m, 3H), 2.05–2.12 (dd, J = 9.0, 12.4 Hz, 1H), 2.98–3.03 (dd, J = 4.8, 8.9 Hz, 1H), 4.25 (s, 1H), 4.42 (s, 1H), 7.87 (d, J = 8.3 Hz, 2H), 7.98 (dd, J = 9.6, 2.6 Hz, 1H), 8.11 (d, J = 8.4 Hz, 2H), 8.16 (s, 1H); ^{13}C NMR ($CDCl_3$) δ (ppm) 28.3 (3C), 28.8, 29.6, 40.7, 44.7, 56.0, 61.9, 80.0, 117.6, 120.6 (J_{CF} = 28.3 Hz), 121.9, 130.2, 130.2, 130.9, 139.4 (J_{CF} = 3.3 Hz), 140.2 (J_{CF} = 4.9 Hz), 142.7 (J_{CF} = 5.6 Hz), 146.8 (J_{CF} = 15.0 Hz), 154.9, 157.3, 160.5.

[^{3}H]Epibatidine Binding Assay—Adult male rat cerebral cortices (Pelfreeze Biological, Rogers, AK) were homogenized in 39 volumes of ice-cold 50 mM Tris buffer (pH 7.4 at 4 °C) containing 120 mM NaCl, 5 mM KCl, 2 mM $CaCl_2$, and 1 mM $MgCl_2$ and sedimented at 37,000 g for 10 min at 4 °C. The supernatant was discarded, the pellet resuspended in the original volume of buffer, and the wash procedure repeated twice more. After the last centrifugation, the pellet was resuspended in 1/10 its original homogenization volume and stored at −80 °C until needed. In a final volume of 0.5 mL, each assay tube contained 3 mg wet weight male rat cerebral cortex homogenate (added last), 0.5 nM [^{3}H]epibatidine (NEN Life Science Products, Wilmington, DE) and one of 10–12 different concentrations of test compound dissolved in buffer (pH 7.4 at room temperature) containing 10% DMSO resulting in a final DMSO concentration of 1%. Total and nonspecific bindings were determined in the presence of vehicle and 300 μM (−)-nicotine, respectively. After a 4-h incubation period at room temperature, the samples were vacuum-filtered over GF/B filter papers presoaked in 0.03% polyethylenimine using a Brandel 48-well harvester and washed with 6 mL of ice-cold buffer. The amount of radioactivity trapped on the filter was determined by standard liquid scintillation techniques in a TriCarb 2200 scintillation counter (Packard Instruments, Meriden, CT) at approximately 50% efficiency. The binding data were fit using the nonlinear regression analysis routines in Prism (Graphpad, San Diego, CA). The K_i values for the test compounds were calculated from their respective IC_{50} values using the Cheng-Prusoff equation.

[^{125}I]Iodo-MLA Binding Assay—Adult male rat cerebral cortices (Pel-Freez Biologicals, Rogers, AK) were homogenized (polytron) in 39 volumes of ice-cold 50 mM Tris buffer (assay buffer; pH 7.4 at 4 °C) containing 120 mM NaCl, 5 mM KCl, 2 mM $CaCl_2$, and 1 mM $MgCl_2$. The homogenate was centrifuged at 35,000 g for 10 min at 4 °C and the supernatant discarded. The pellet was resuspended in the original volume of buffer and the wash procedure repeated twice more. After the last centrifugation step, the pellet was resuspended in one-tenth the original homogenization volume and stored at −80 °C until needed. Triplicate samples were run in 1.4-mL polypropylene tubes (Matrix Technologies Corporation, Hudson, NH). Briefly, in a final volume of 0.5 mL, each assay sample contained 3 mg wet weight rat cerebral cortex (added last), 40–50 pM [^{125}I]MLA and 50 nM final concentration of test compound dissolved in buffer containing 10% DMSO, giving a final DMSO concentration of 1%. Total and nonspecific binding were determined in the presence of vehicle and 300 μM (−)-nicotine, respectively. After a 2-h incubation period on ice, the samples were vacuum-filtered using a Multimate 96-well harvester (Packard Instruments, Meriden, CT) onto GF/B filters presoaked for at least 30 min in assay buffer containing 0.15% bovine serum albumin. Each well was then washed with approximately

3.0 mL of ice-cold buffer. The filter plates were dried, and 30 μL of Microscint20 (Packard) was added to each well. The amount of radioligand remaining on each filter was determined using a TopCount 12-detector (Packard) microplate scintillation counter at approximately 70% efficiency.

Tail-flick Test—Antinociception was assessed by the tail-flick method of D'Amour and Smith.[34] A control response (2–4 sec) was determined for each mouse before treatment, and a test latency was determined after drug administration. In order to minimize tissue damage, a maximum latency of 10 sec was imposed. Antinociceptive response was calculated as percent maximum possible effect (% MPE), where %MPE = [(test-control)/(10-control)] × 100. Groups of eight to twelve animals were used for each dose and for each treatment. The mice were tested 5 min after s.c. injections of epibatidine analogues for the dose-response evaluation. Eight to twelve mice were treated per dose and a minimum of four doses were performed for dose-response curve determination.

Hot-plate Test—Mice were placed into a 10 cm wide glass cylinder on a hot plate (Thermojust Apparatus) maintained at 55 °C. Two control latencies at least 10 min apart were determined for each mouse. The normal latency (reaction time) was 8 to 12 sec. Antinociceptive response was calculated as percent maximum possible effect (% MPE), where %MPE = [(test-control)/40-control) × 100]. The reaction time was scored when the animal jumped or licked its paws. Eight mice per dose were injected s.c. with epibatidine analogues and tested 5 min thereafter in order to establish a dose-response curve.

Locomotor Activity—Mice were placed into individual Omnitech photocell activity cages (28 × 16.5 cm) 5 min after s.c. administration of either 0.9% saline or epibatidine analogues. Interruptions of the photocell beams (two banks of eight cells each) were then recorded for the next 10 min. Data were expressed as number of photocell interruptions.

Body Temperature—Rectal temperature was measured by a thermistor probe (inserted 24 mm) and digital thermometer (Yellow Springs Instrument Co., Yellow Springs, OH). Readings were taken just before and 30 min at different times after the s.c. injection of either saline or epibatidine analogues. The difference in rectal temperature before and after treatment was calculated for each mouse. The ambient temperature of the laboratory varied from 21–24 °C from day to day.

Electrophysiology—*Xenopus laevis* oocytes were surgically obtained, and follicle cells were removed by treatment with collagenase B for 2 h at room temperature. cRNA encoding the rat α3, α4, α7, β2, and β4 neuronal nAChR subunits was synthesized using mMessage mMachine kits (Ambion). Oocytes were injected with 10–40 ng of cRNA in 25–50 nL of water and incubated at 19 °C in modified Barth's saline (88 mM NaCl, 1 mM KCl, 2.4 mM $NaHCO_3$, 0.3 mM $Ca(NO_3)_2$ 0.41 mM $CaCl_2$, 0.82 mM $MgSO_4$, 150 ag/mL ceftazidime, 15 mM HEPES, pH 7.6). For α4β2 and α3β4 receptors, cRNA transcripts encoding each subunit were injected into oocytes at a molar ratio of 1:1. Agonist-induced current responses were measured 2–6 days after cRNA injection using two-electrode voltage clamp in an automated parallel electrophysiology system (OpusExpress 6000A, Molecular Devices). Micropipettes were filled with 3M KCl and had resistances of 0.2–2.0 MΩ. For α4β2 and α3β4 receptors, current responses were recorded at a holding potential of −70 mV, filtered (4-pole, Bessel, low pass) at 20 Hz (−3db) and sampled at 100 Hz. For α7 receptors, current responses were recorded at a holding potential of −40 mV (to minimize the contribution of Ca^{2+}-activated Cl^- channels), filtered (4-pole, Bessel, low pass) at 100 Hz (−3db) and sampled at 500 Hz. Current responses were captured and stored using *OpusXpress 1.1* software (Molecular Devices). Oocytes were perfused at room temperature (20–25 °C) with

ND96 (in mM: 96 NaCl, 2 KCl, 1 $CaCl_2$, 1 $MgCl_2$, 5 HEPES, pH 7.5). Compounds, diluted in ND96, were applied for 15 sec (α4β2 and α3β4) or 5 sec (α7) at a flow rate of 4 mL/min, with 3-min washes between applications. Agonist activity was assessed (Table 1) by comparing the current response to 100 μM of each compound to the mean current response of three preceding applications of acetylcholine, applied at an EC_{20} concentration (20 μM for α4β2, 110 μM for α3β4) or an EC_{50} concentration (300 μM for α7). Agonist activity of each compound is expressed as a percentage of the maximal response to acetylcholine. Antagonist activity was initially assessed (Table 1) by comparing the current response to an EC_{50} concentration of acetylcholine (70 μM for α4β2, 200 μM for α3β4, 300 μM for α7) in the presence of 100 μM of each compound to the mean current response of three preceding applications of acetylcholine (EC_{50} concentration). The antagonist activity of some compounds was assessed in more detail (Table 2) by generating concentration-inhibition curves. Data were fit (*Prism 5*, Graphpad) to the equation: $I=I_{max}/[1+(IC_{50}/X)^n]$, where I is the current response at agonist concentration (X), I_{max} is the maximum current, IC_{50} is the ligand concentration producing half-maximal inhibition of the current response, and n is the Hill coefficient.

Molecular Modeling—Ligand-receptor docking simulations were performed performed using Tripos Sybyl-X (version 2.01) running on an eight-core Macintosh workstation. Ligand models were built using the Sybyl fragment library and energy-minimized using the Tripos force-field and Gasteiger-Marsili charges.

The receptor structure used for the docking studies was the X-ray crystallographic coordinates of a human α7-nicotinic receptor – mollusk (*Lymnaea stagnalis*) acethylcholine binding protein chimera complexed with epibatidine (PDB:3SQ6). The "A" and "B" subunits of 3SQ6 and the associated ligand (epibatidine) were selected for the calculations. AMBER7 FF99 (biopolymer) and Gasteiger-Marsili (ligand) charges were applied to the receptor-ligand complex in preparation for use in docking studies. The Surflex "protomol" was generated based on the X-ray coordinates of the bound ligand with a threshold parameter of 0.5 and "bloat" value of 4.

The Surflex-Dock calculations were performed with default parameters plus options selected for full flexibility of both the ligand and the receptor ligand binding domain. Twenty poses for each ligand were examined and, based on the Surflex "total score" (an estimated −log(Kd)) the optimal pose for each ligand was selected. A post-dock minimization was performed for both the ligand and receptor and a final score was calculated based on this optimized docked structure.

Supplementary Material

Refer to Web version on PubMed Central for supplementary material.

Acknowledgments

This research was supported by the National Institute on Drug Abuse Grant No. DA12001.

ABBREVIATIONS USED

Ls-AChBP	*Lymnaea stagnalis* acetylcholine binding protein
NRT	nicotine replacement therapy
CDC	Centers for Disease Control

nAChR	nicotinic acetylcholine receptor
AChBP	acetylcholine binding protein
ICSS	intracranial self-stimulation
CPP	conditioned place preference
DD	drug discrimation
SA	self-administration
$PdCl_2$(dppf)	1,1'-bis(diphenylphosphino)ferrocene-palladium(II) dichloride
MCPBA	*meta*-chloroperoxybenzoic acid
MPE	maximum potential effect
DHβE	dihydro-β-erythroidine

REFERENCES

1. Centers for Disease Control and Prevention. Centers for Disease Control and Prevention, Smoking and Tobacco Use-Fact Sheet: Smoking Cessation (updated November 2011). http://www.cdc.gov/tobacco/data_statistics/fact_sheets/cessation/quitting/index.htm
2. Dwoskin LP, Smith AM, Wooters TE, Zhang Z, Crooks PA, Bardo MT. Nicotinic receptor-based therapeutics and candidates for smoking cessation. Biochem. Pharmacol. 2009; 78:732–743. [PubMed: 19523455]
3. Fowler CD, Arends MA, Kenny PJ. Subtypes of nicotinic acetylcholine receptors in nicotine reward, dependence, and withdrawal: evidence from genetically modified mice. Behav. Pharmacol. 2008; 19:461–484. [PubMed: 18690103]
4. Russo P, Cesario A, Rutella S, Veronesi G, Spaggiari L, Galetta D, Margaritora S, Granone P, Greenberg DS. Impact of genetic variability in nicotinic acetylcholine receptors on nicotine addiction and smoking cessation treatment. Curr. Med. Chem. 2011; 18:91–112. [PubMed: 21110812]
5. Joslyn G, Brush G, Robertson M, Smith TL, Kalmijn J, Schuckit M, White RL. Chromosome 15q25.1 genetic markers associated with level of response to alcohol in humans. Proc Natl Acad Sci U S A. 2008; 105:20368–20373. [PubMed: 19064933]
6. Saccone NL, Wang JC, Breslau N, Johnson EO, Hatsukami D, Saccone SF, Grucza RA, Sun L, Duan W, Budde J, Culverhouse RC, Fox L, Hinrichs AL, Steinbach JH, Wu M, Rice JP, Goate AM, Bierut LJ. The CHRNA5-CHRNA3-CHRNB4 nicotinic receptor subunit gene cluster affects risk for nicotine dependence in African-Americans and in European-Americans. Cancer Res. 2009; 69:6848–6856. [PubMed: 19706762]
7. Wang HY, Lee DH, D'Andrea MR, Peterson PA, Shank RP, Reitz AB. beta-Amyloid(1-42) binds to alpha7 nicotinic acetylcholine receptor with high affinity. Implications for Alzheimer's disease pathology. J. Biol. Chem. 2000; 275:5626–5632. [PubMed: 10681545]
8. Frahm S, Slimak MA, Ferrarese L, Santos-Torres J, Antolin-Fontes B, Auer S, Filkin S, Pons S, Fontaine JF, Tsetlin V, Maskos U, Ibanez-Tallon I. Aversion to nicotine is regulated by the balanced activity of beta4 and alpha5 nicotinic receptor subunits in the medial habenula. Neuron. 2011; 70:522–535. [PubMed: 21555077]
9. Gallego X, Molas S, Amador-Arjona A, Marks MJ, Robles N, Murtra P, Armengol L, Fernandez-Montes RD, Gratacos M, Pumarola M, Cabrera R, Maldonado R, Sabria J, Estivill X, Dierssen M. Overexpression of the CHRNA5/A3/B4 genomic cluster in mice increases the sensitivity to nicotine and modifies its reinforcing effects. Amino Acids. 2011
10. Toll L, Zaveri NT, Polgar WE, Jiang F, Khroyan TV, Zhou W, Xie XS, Stauber GB, Costello MR, Leslie FM. AT-1001: A High Affinity and Selective α3β4 Nicotinic Acetylcholine Receptor Antagonist Blocks Nicotine Self-Administration in Rats. Neuropsychopharmacology. 2012; 37:1367–1376. [PubMed: 22278092]

11. Chatterjee S, Steensland P, Simms JA, Holgate J, Coe JW, Hurst RS, Shaffer CL, Lowe JA, Rollema H, Bartlett SE. Partial agonists of the a3b4* neuronal nicotinic acetylcholine receptor reduce ethanol consumption and seeking in rats. Neuropsychopharmacology. 2011; 36:603–615. [PubMed: 21048701]
12. Johnston AJ, Ascher J, Leadbetter R, Schmith VD, Patel DK, Durcan M, Bentley B. Pharmacokinetic optimisation of sustained-release bupropion for smoking cessation. Drugs. 2002; 62(Suppl 2):11–24. [PubMed: 12109932]
13. Hesse LM, Venkatakrishnan K, Court MH, von Moltke LL, Duan SX, Shader RI, Greenblatt DJ. CYP2B6 mediates the in vitro hydroxylation of bupropion: potential drug interactions with other antidepressants. Drug Metab. Dispos. 2000; 28:1176–1183. [PubMed: 10997936]
14. Carroll FI, Ma W, Deng L, Navarro HA, Damaj MI, Martin BR. Synthesis, Nicotinic Acetylcholine Receptor Binding, and Antinociceptive Properties of 3'-(Substituted Phenyl)epibatidine Analogues. Nicotinic Partial Agonists. J. Nat. Prod. 2010; 73:306–312. [PubMed: 20038125]
15. Carroll FI, Yokota Y, Ma W, Lee JR, Brieaddy LE, Burgess JP, Navarro HA, Damaj MI, Martin BR. Synthesis, nicotinic acetylcholine receptor binding, and pharmacological properties of 3'-(substituted phenyl)deschloroepibatidine analogs. Bioorg. Med. Chem. 2008; 16:746–754. [PubMed: 17964169]
16. Carroll FI, Ma W, Yokota Y, Lee JR, Brieaddy LE, Navarro HA, Damaj MI, Martin BR. Synthesis, nicotinic acetylcholine receptor binding, and antinociceptive properties of 3'-substituted deschloroepibatidine analogues. Novel nicotinic antagonists. J. Med. Chem. 2005; 48:1221–1228. [PubMed: 15715488]
17. Carroll FI, Ware R, Brieaddy LE, Navarro HA, Damaj MI, Martin BR. Synthesis, nicotinic acetylcholine receptor binding, and antinociceptive properties of 2'-fluoro-3'-(substituted phenyl)deschloroepibatidine analogs. Novel nicotinic antagonist. J. Med. Chem. 2004; 47:4588–4594. [PubMed: 15317468]
18. Carroll FI, Lee JR, Navarro HA, Ma W, Brieaddy LE, Abraham P, Damaj MI, Martin BR. Synthesis, nicotinic acetylcholine receptor binding, and antinociceptive properties of 2-exo-2-(2', 3'-disubstituted 5'-pyridinyl)-7-azabicyclo[2.2.1]heptanes: epibatidine analogues. J. Med. Chem. 2002; 45:4755–4761. [PubMed: 12361403]
19. Carroll FI, Lee JR, Navarro HA, Brieaddy LE, Abraham P, Damaj MI, Martin BR. Synthesis, nicotinic acetylcholine receptor binding, and antinociceptive properties of 2-exo-2-(2'-substituted-3'-phenyl-5'-pyridinyl)-7-azabicyclo[2.2.1]heptanes. Novel nicotinic antagonist. J. Med. Chem. 2001; 44:4039–4041. [PubMed: 11708907]
20. Carroll FI, Liang F, Navarro HA, Brieaddy LE, Abraham P, Damaj MI, Martin BR. Synthesis, nicotinic acetylcholine receptor binding, and antinociceptive properties of 2-exo-2-(2'-substituted 5'-pyridinyl)-7-azabicyclo[2.2.1]heptanes. Epibatidine analogues. J. Med. Chem. 2001; 44:2229–2237. [PubMed: 11405659]
21. Abdrakhmanova GR, Damaj MI, Carroll FI, Martin BR. 2-Fluoro-3-(4-nitrophenyl) deschloroepibatidine is a novel potent competitive antagonist of human neuronal α4β2 nAChRs. Mol. Pharmacol. 2006; 69:1945–1952. [PubMed: 16505153]
22. Tobey KM, Walentiny DM, Wiley JL, Carroll FI, Damaj MI, Azar MR, Koob GF, George O, Harris LS, Vann RE. Effects of the Specific α4β2 nAChR Antagonist, 2-Fluoro-3-(4-nitrophenyl)deschloroepibatidine, on Nicotine Reward-related Behaviors. Psychopharmacology (Berl). 2012
23. Li SX, Huang S, Bren N, Noridomi K, Dellisanti CD, Sine SM, Chen L. Ligandbinding domain of an alpha7-nicotinic receptor chimera and its complex with agonist. Nat Neurosci. 2011; 14:1253–1259. [PubMed: 21909087]
24. SYBYL-X 1.2. 1699 South Hanley Road: St. Louis, MO 63144, USA: Tripos International;
25. Huang Y, Zhu Z, Xiao Y, Laruelle M. Epibatidine analogues as selective ligands for the alpha(x)beta2-containing subtypes of nicotinic acetylcholine receptors. Bioorg. Med. Chem. Lett. 2005; 15:4385–4388. [PubMed: 16039849]
26. Carroll FI. Epibatidine Structure-Activity Relationships. Bioorg. Med. Chem. Lett. 2004; 14:1889–1896. [PubMed: 15050621]

27. Hansch, C.; Leo, A. Exploring QSAR: Fundamenetals and Applications in Chemistry and Biology. Washington, DC: American Chemical Society; 1995. Electronic Effects on Organic Reactions; p. 7

28. Stokes C, Papke JK, Horenstein NA, Kem WR, McCormack TJ, Papke RL. The structural basis for GTS-21 selectivity between human and rat nicotinic alpha7 receptors. Mol Pharmacol. 2004; 66:14–24. [PubMed: 15213292]

29. Coe JW, Brooks PR, Vetelino MG, Wirtz MC, Arnold EP, Huang J, Sands SB, Davis TI, Lebel LA, Fox CB, Shrikhande A, Heym JH, Schaeffer E, Rollema H, Lu Y, Mansbach RS, Chambers LK, Rovetti CC, Schulz DW, Tingley FD 3rd, O'Neill BT. Varenicline: an α4β2 nicotinic receptor partial agonist for smoking cessation. J. Med. Chem. 2005; 48:3474–3477. [PubMed: 15887955]

30. Mihalak KB, Carroll FI, Luetje CW. Varenicline Is a Partial Agonist at {alpha}4beta2 and a Full Agonist at {alpha}7 Neuronal Nicotinic Receptors. Mol. Pharmacol. 2006; 70:801–805. [PubMed: 16766716]

31. Avalos M, Parker MJ, Maddox FN, Carroll FI, Luetje CW. Effects of pyridine ring substitutions on the affinity, efficacy, and subtype selectivity of the neuronal nicotinic receptor agonist epibatidine. J. Pharmacol. Exp. Ther. 2002; 302:1246–1252. [PubMed: 12183686]

32. Jensen AA, Frolund B, Liljefors T, Krogsgaard-Larsen P. Neuronal nicotinic acetylcholine receptors: structural revelations, target identifications, and therapeutic inspirations. J Med Chem. 2005; 48:4705–4745. [PubMed: 16033252]

33. Navarro HA, Xu H, Zhong D, Abraham P, Carroll FI. In vitro and In vivo characterization of [^{125}I]iodomethyllycaconitine in the rat. Synapse. 2002; 44:117–123. [PubMed: 11954042]

34. D'Amour FE, Smith DL. A method for determining loss of pain sensation. J. Pharmacol. Exp. Ther. 1941; 72:74–79.

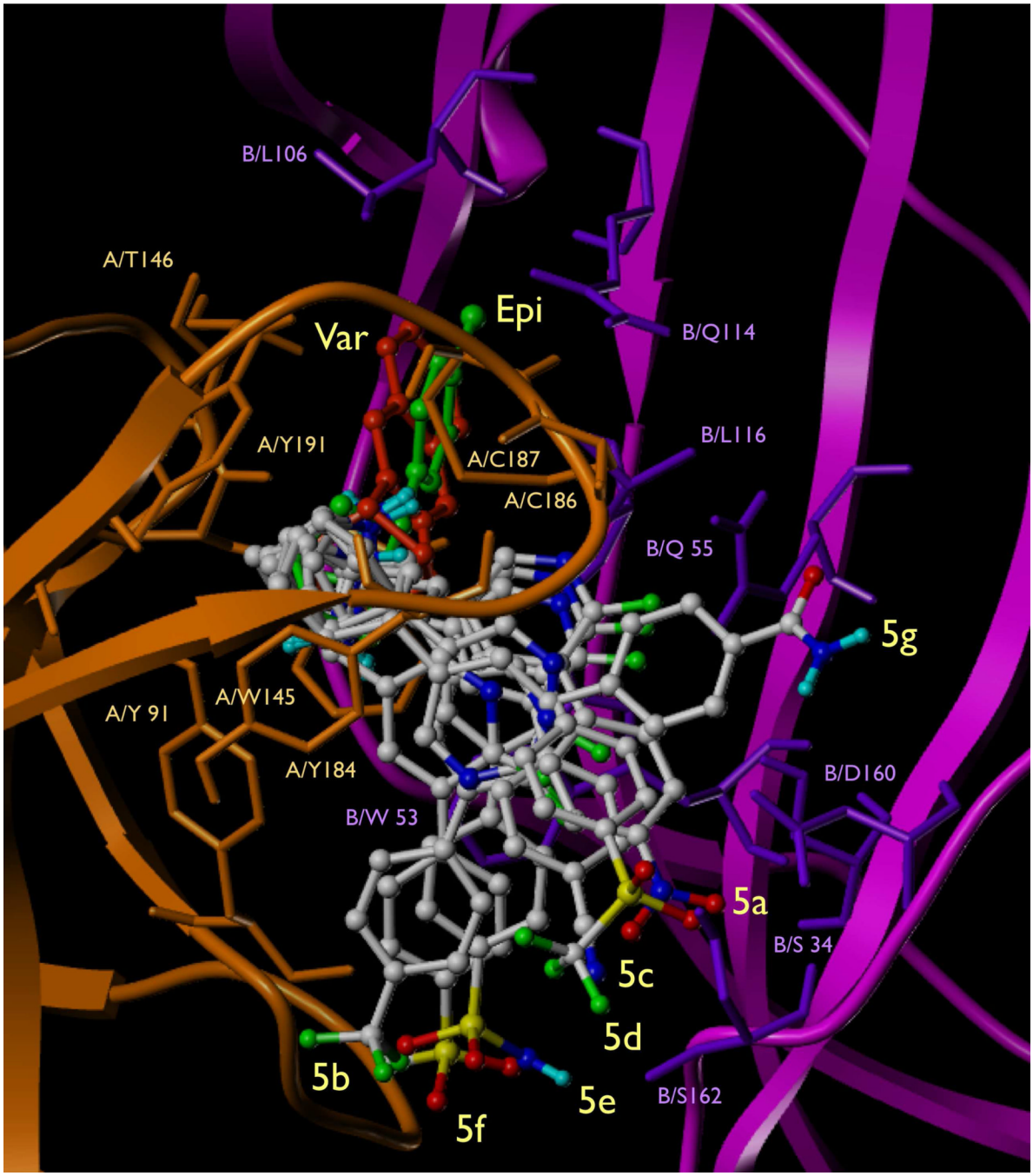

Figure 1.

Overlay of the calculated docking geometries of **5a–5g** and varenicline overlayed with the observed X-ray crystallographic structure of epibatidine co-crystallized with an α7-AChBP chimera (PDB: 3SQ6). The "A" subunit of the receptor (the C-loop region) is colored orange, the "B" subunit purple. Epibatidine is colored green, varenicline red, and the **5a–5g** epibatidine analogs are rendered with CPK atom-type colors.

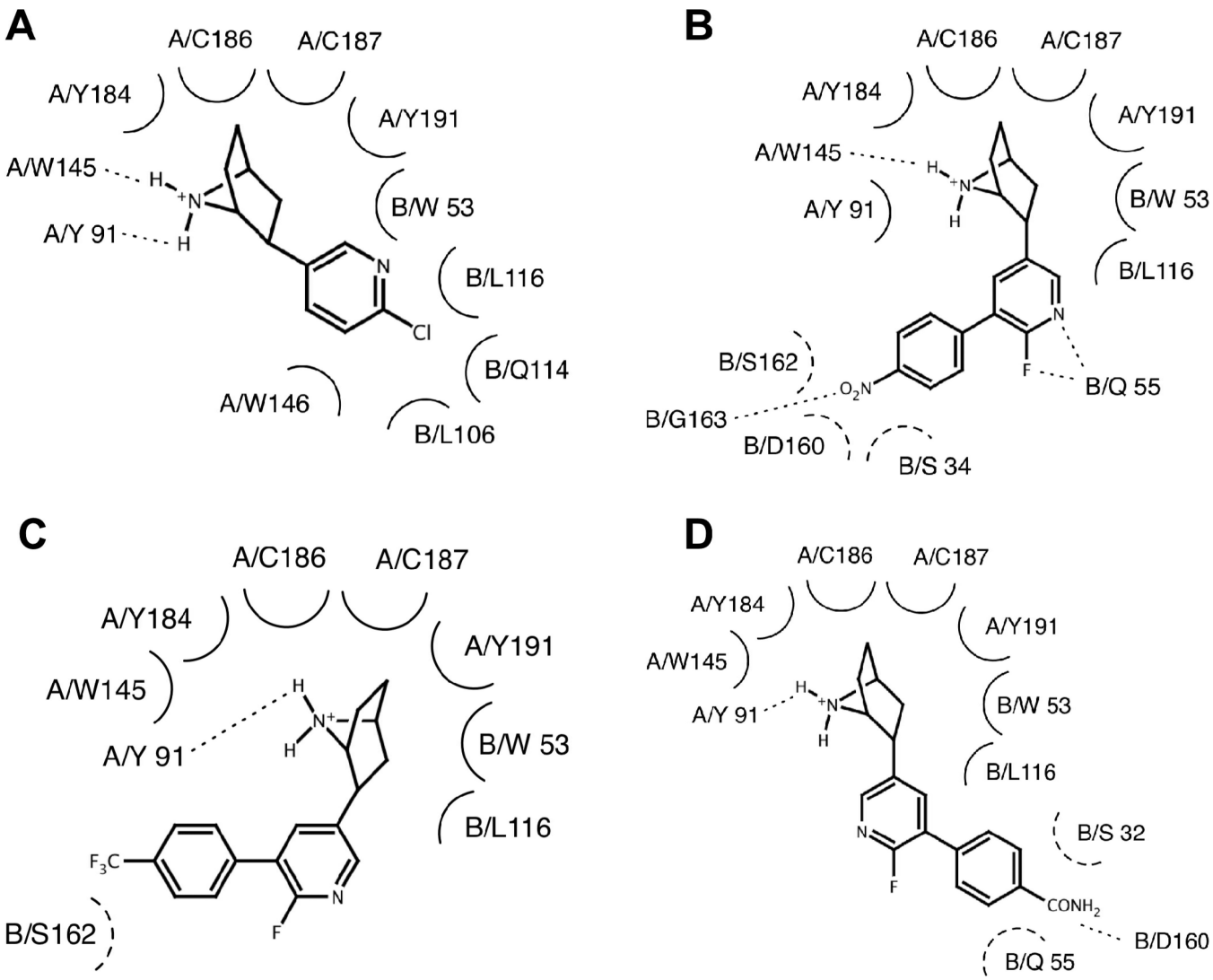

Figure 2.

Diagrams of the salient ligand-receptor close contacts (5 Å cut-off) for epibatidine (observed), and **5a–5g** and varenicline (calculated). (A) Binding Mode 1 (epibatidine and varenicline); (B) Binding Mode 2 (Analogues **5a, 5c**, and **5d**); (C) Binding Mode 3 (Analogues **5b, 5e**, and **5f**); (D) Binding Mode 4 (Analogue **5g**).

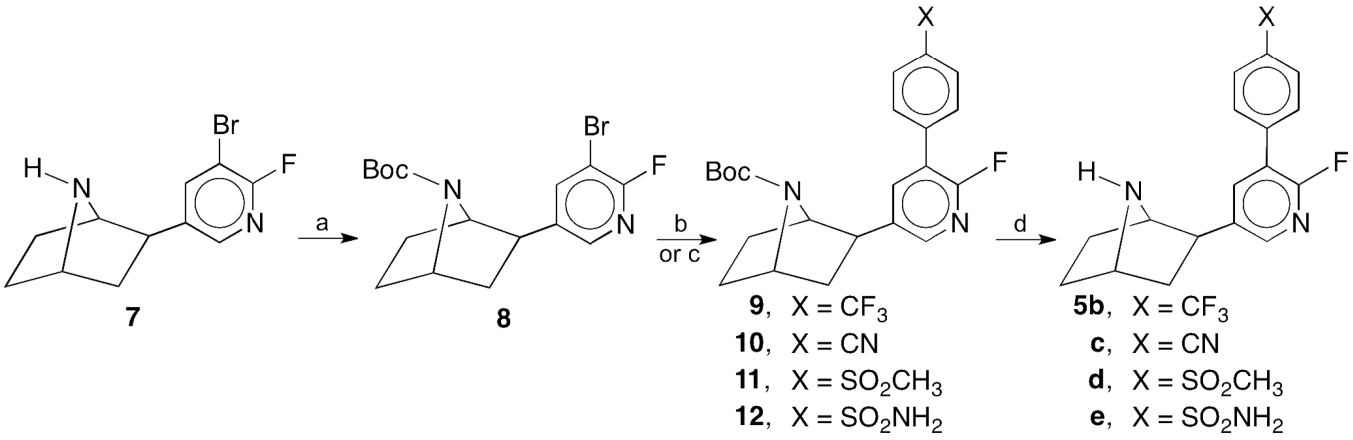

Scheme 1.

[a] Reagents and conditions: (a) $(Boc)_2O$, Et_3N, CH_2Cl_2, rt, overnight; (b) $Pd(OAc)_2$, P(*o*-tolyl)$_3$, Na_2CO_3, DME, H_2O, 85 °C, X-C$_6$H$_4$-$B(OH)_2$ (X = CF_3, CN, or SO_2CH_3); (c) $PdCl_2$(dppf), K_2CO_3, 1,4-dioxane, H_2O, μw, 140 °C, 20 min; (d) CF_3CO_2H, CH_2Cl_2.

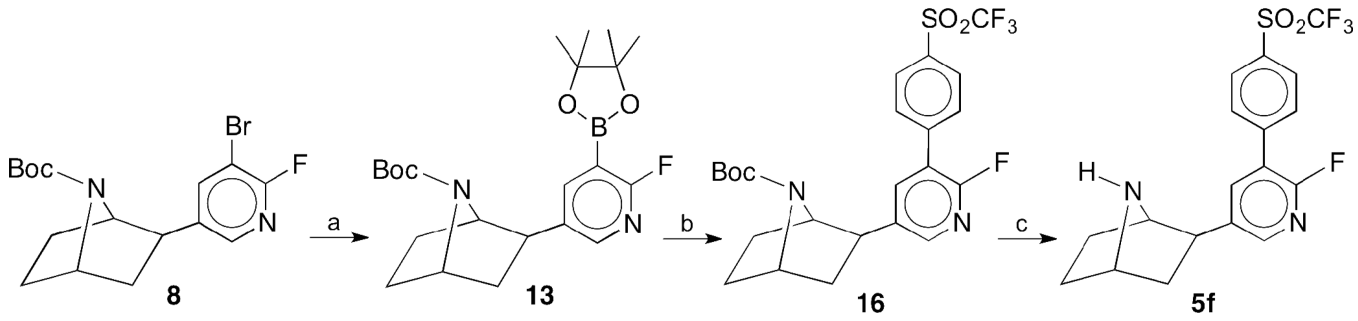

Scheme 2.

[a] Reagents and conditions: (a) Bis(pinacolato)diboron, KOAc, $PdCl_2$(dppf), 1,4-dioxane, μw 140 °C, 20 min; (b) $Pd(PPh_3)_4$, K_2CO_3, DME-EtOH-H_2O, μw, 140 °C, 20 min, 4-$BrC_6H_4SO_2CF_3$ (**15**) (prepared by oxidation of 4-Br-$C_6H_4SCF_3$ (**14**) with MCPBA); (c) CF_3CO_2H, CH_2Cl_2.

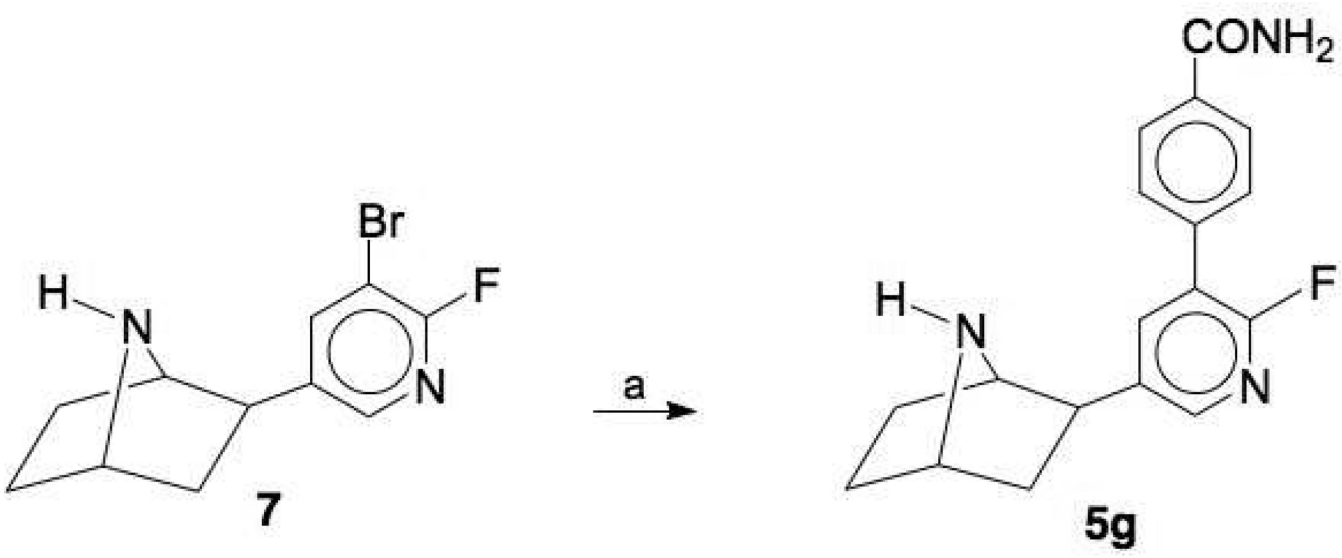

Scheme 3.

[a] Reagents and conditions: (a) $Pd(PPh_3)_4$, K_2CO_3, 1,4-dioxane; H_2O, reflux, 24 h with 4-carbamoylphenylboronic acid.

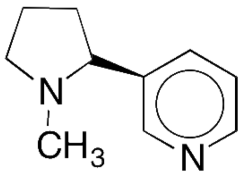

1

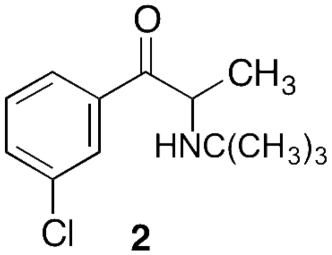

2

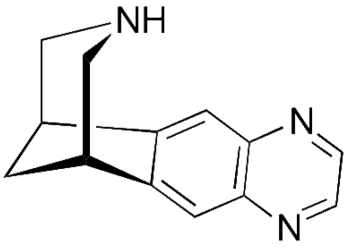

3

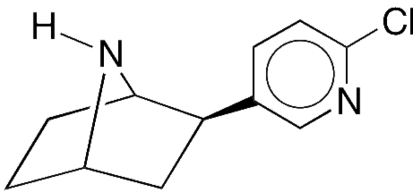

4

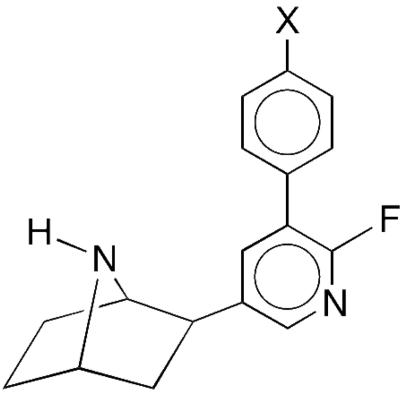

5a, X = NO_2
b, X = CF_3
c, X = CN
d, X = SO_2CH_3
e, X = SO_2NH_2
f, X = SO_2CF_3
g, X = $CONH_2$

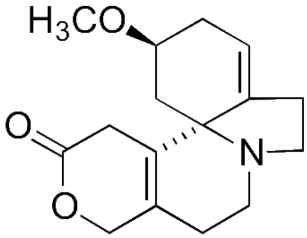

6

Table 1

Comparison of Epibatidine and Varenicline Radioligand Binding, Antinociception, and In Vitro Functional Data to 2'-Fluoro-3'-(substituted phenyl)deschloroepibatidine Analogs.

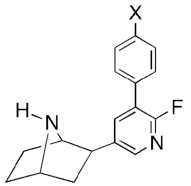

Compd[a]	X	αβ[b] [^{3}H]-Epibatidine (K_i, nM) (Hill slope)	α$_7$ [^{125}I]-iodoMLA (K_i, nM) (Hill slope)	mg/kg				AD$_{50}$ (μg/kg)		Agonist Activity (% of max ACh at 100 μM of Compd)			Antagonist Activity (% EC$_{50}$ Ach Response Remaining at 100 μM of Compd)		
				ED$_{50}$ Tail-Flick	ED$_{50}$ Hot-Plate	ED$_{50}$ Hypothermia	ED$_{50}$ Spontaneous Activity	Tail-Flick	Hot-Plate	α4β2	α3β4	α7	α4β2	α3β4	α7
nat-epibatidine		0.026 ± 0.002		0.006 (0.001–0.01)	0.004 (0.001–0.008)	0.004 (0.002–0.008)	0.001 (0.0005–0.005)			131 ± 13	97 ± 4	150 ± 8	nd	nd	nd
varenicline		0.12 ± 0.02	32.5 ± 1.3	11% @ 10	10% @ 10	2.8	2.1	0.2	470	13 ± 0.4	66 ± 4	74 ± 5	38 ± 2	nd	nd
5a	NO_2	0.009 ± 0.001	>2000	5% @ 10	10% @ 10	0.21 (0.4–1.9)	0.22 (0.04–1.2)	3 (0.8–45)	120 (10–900)	0	4 ± 1	6 ± 1	6 ± 1	9 ± 2	55 ± 6
5b	CF_3	0.44 ± 0.05	>2000	4% @ 10	6% @ 10	0% @ 10	5% @ 10	38 (2–50)	6000 (4100–8800)	0	0	4 ± 1	8 ± 2	4 ± 1	3 ± 1
5c	CN	0.19 ± 0.012	>2000	4% @ 10	18% @ 10	0% @ 10	0% @ 10	6 (3–100)	24% @ 10000	0	6 ± 1	3 ± 1	8 ± 2	17 ± 2	49 ± 5
5d	CH_3SO_2	0.17 ± 0.027	>2000	6% @ 10	1% @ 10	1% @ 10	12% @ 10	18 (2–160)	2600 (1100–5800)	0	0	3 ± 1	10 ± 3	25 ± 5	33 ± 2
5e	H_2NSO_2	0.94 ± 0.061	>2000	4% @ 10	19% @ 10	0% @ 10	5% @ 10	0.9 (0.4–1.8)	1000 (100–1800)	0	0	1.8 ± 0.5	4 ± 1	5 ± 2	18 ± 2
5f	CF_3SO_2	0.03 ± 0.004	>2000	3% @ 10	15% @ 10	0% @ 10	4.2 (1–16)	1600 (1500–1800)	50% @ 10000	0	1.9 ± 0.6	1.8 ± 0.4	7 ± 2	15 ± 5	42 ± 5
5g	$CONH_2$	0.12 ± 0.021	1870 ± 298	16% @ 10	60% @ 10	4.2 (1.5–11.6)	3.5 (1–11.3)	9 (3–31)	1% @ 2000	3.5 ± 1.1	8 ± 1	17 ± 4	6 ± 1	36 ± 4	54 ± 5

J Med Chem. Author manuscript; available in PMC 2013 July 26.

[a] All compounds were tested as their (±)-isomers.

[b] The K_d for (±)-[^{3}H]epibatidine is 0.02 nM.

Table 2

Comparison of Antagonist Potency (IC_{50} values) for Several 2'-Fluoro-3'-(substituted phenyl)deschloroepibatidine Analogues

Compd	Antagonist Activity IC_{50}, μM		
	α4β2	α3β4	α7
varenicline	0.20 ± 0.03[a]		
5a	3.2 ± 0.2	7.9 ± 0.5	32 ± 12
5b	6.0 ± 0.4	5.0 ± 0.3	4.0 ± 0.8
5c	11 ± 1	7 ± 7	98 ± 13
5d	2.8 ± 0.4	11 ± 2	19 ± 7
5g	1.5 ± 0.1	35 ± 7	35 ± 12

[a]Data were taken from ref. 29.

Table 3

Comparison of Representative σ Constants Derived from Different Systems[a]

Substituent	σ_m	σ_p	σ_p^0	σ_p^+	σ_p^-	R	F[a]
NO_2	0.71	0.78	0.82	0.79	1.27	0.13	0.65
SO_2NH_2	0.53	0.60	—	—	0.94	0.11	0.49
CF_3	0.43	0.54	0.54	0.61	0.65	016	0.38
SO_2CF_3	0.86	0.96	0.93	—	1.63	0.22	0.74
CN	0.56	0.66	0.68	0.66	1.00	0.15	0.51
$CONH_2$	0.28	0.36	—	—	0.61	0.10	0.26
SO_2CH_3	0.60	0.72	0.75	—	1.13	0.19	0.53

[a]Data were taken from ref. 26.